IEEE Access
Multidisciplinary | Rapid Review | Open Access Journal

Received December 1, 2019, accepted December 18, 2019, date of publication December 26, 2019, date of current version June 3, 2020.

Digital Object Identifier 10.1109/ACCESS.2019.2962529

Optimal Design and Experimental Research on a New Hybrid Electromagnetic Actuator for Vehicles

XIANGPENG MENG, RUOCHEN WANG, RENKAI DING, AND LONG CHEN
School of Automotive and Traffic Engineering, Jiangsu University, Zhenjiang 212013, China

Corresponding author: Xiangpeng Meng (mengxp@ujs.edu.cn)

This work was supported in part by the National Natural Science Foundation Project, China, under Project 51970523, and in part by the Key Laboratory for New Technology Application of Road Conveyance of Jiangsu Province under Grant BM20082061710.

ABSTRACT In this study, a new hybrid electromagnetic actuator (HEMA) that integrates a cylindrical permanent magnet linear synchronous motor and a hydraulic damper is proposed and designed to solve the problem of poor reliability of a linear electromagnetic actuator. A modified skyhook control that matches the structure of the HEMA is adopted, and the performance parameters are optimized. Then, the relationships among structural parameters of the HEMA are analyzed using equivalent magnetic circuit method. On the basis of these relationships, multiple alternative groups of structural parameters are obtained. Moreover, finite element models are established in Ansoft Maxwell software. The structural parameters of the HEMA are optimized and determined to produce the peak electromagnetic thrust force that the linear motor requires. Finally, a prototype is developed on the basis of the optimized results for the bench test. Test results show that the linear motor tracks the desired force effectively. In contrast to the passive damper, the body acceleration and suspension working space of HEMA are decreased by 20.6% and 13.3%, respectively. The dynamic tire load is increased by 16%, which is in a reasonable range. And compared with LEMA, the body acceleration is increased by 2.73%, but the suspension working space and dynamic tire load are reduced by 1.1% and 38.1%. All the results above mentioned demonstrate that the HEMA can considerably improve the vehicle dynamic performance.

INDEX TERMS Hybrid electromagnetic actuator, modified skyhook control strategy, optimal design, experimental research.

I. INTRODUCTION

Traditional vehicle passive suspension systems cannot meet the increasing requirements for riding comfort and driving safety of vehicles. However, the active suspension can adjust the stiffness and damping of suspension to obtain great riding comfort and driving safety according to road conditions. Thus, active suspension has become a new trend of development. Moreover, the performance of actuators, which are important components of an active suspension system, has a direct influence on the functions of active suspension. Simultaneously, given the rapid development of motor technology, many scholars have applied them in designing electromagnetic actuators for active suspension [1]–[3].

The associate editor coordinating the review of this manuscript and approving it for publication was Jinquan Xu.

At present, some scholars have designed rotary electromagnetic actuators using rotary motors. Montazerigh designed a rotary electromagnetic actuator that combined a rotary motor with a ball screw, applied it in the hybrid electric vehicle, and studied the effect of the actuator on the performance of suspension on the basis of a hybrid control strategy that united skyhook and ground-hook control [4]–[6]. Singal also developed the same structure of actuator and analyzed the possibility of self-powered suspension on the basis of an adaptive skyhook control strategy [7]. Zuo adopted rack-and-pinion and rotary motor for an actuator and verified its performance via simulation and test [8], [9]. The aforementioned scholars have made considerable research on the rotary electromagnetic actuator. However, when a rotary motor is used for the actuator, an additional transmission (i.e., rack and pinion/ball screw) is essential to convert the

linear vibration into rotary motion, thereby complicating the suspension system. Moreover, the inherent rotary inertia limits the response capability to the high-frequency reciprocating motion. In comparison with rotary motor, linear motor possesses a simple structure, elicits rapid response, and yields large controllable bandwidth. Hence, some scholars have introduced linear motors in suspension systems to design linear electromagnetic actuators (LEMAs). Martins used a two-phase axially magnetized cylindrical permanent magnet (PM) linear motor to design a LEMA and conducted a test to verify that the actuator could output active force required by suspension [10]. Bart applied an electromagnetic actuator made of PM brushless linear motor to MacPherson suspension of BMW 530i and conducted a test that showed that the actuator could track the damping force of the passive suspension well [11]–[13]. Tang designed an electromagnetic actuator using an axially magnetized PM synchronous linear motor and analyzed the mechanism of the motor [14]. However, when a single linear motor is used to replace the hydraulic damper of traditional passive suspension, the reliability of the suspension system cannot be guaranteed. That is, once the supply power or control circuit is faulty, the active control fails and the passive control works. Furthermore, the linear motor is equivalent to an electromagnetic damper. However, the damping force resulting from the eddy current effect is ''soft damping'', which is considerably less than that of the hydraulic damper, thereby affecting the performance of suspension; thus, when the linear motor functions as an electromagnetic damper, it cannot attenuate the vibration rapidly. To address the reliability-related problem, a few scholars have introduced passive damping and constituted a ''linear motor–damper'' hybrid electromagnetic actuator (HEMA). Thus, adding a passive damper can improve the reliability of the suspension system. Moreover, passive damping can reduce the performance demand of suspension systems for linear motors, such as, peak electromagnetic thrust force, thereby reducing the output power of linear motors and achieving energy reduction. Babak used a linear motor that adopted a double-layer PM to design an electromagnetic actuator that could increase eddy current damping [15]–[17]. Asadi integrated a linear motor and a hydraulic damper in designing a HEMA; this HEMA placed the linear motor inside the hydraulic damper to replace the piston assembly, in which base damping was provided by the hydraulic damper [18]–[20]. Moreover, the linear motor was used to regenerate the vibration energy. However, this structure was complex and difficult to develop. Furthermore, given that the linear motor was inside the hydraulic damper, the performance of PM would be affected by the high temperature of the hydraulic oil, thereby possibly influencing the functions of the actuator.

Thus, on the basis of the current research results and related problems, the present study proposes a new HEMA that integrates a linear motor and a hydraulic damper. The linear motor is placed outside the hydraulic damper to reduce the difficulty of development. In comparison with LEMA, this new HEMA can realize the effect of energy saving and improve the reliability of the suspension system. Moreover, to verify the effectiveness of this new HEMA, a prototype is developed on the basis of the optimization of performance and structural parameters, and a bench test is conducted on it.

The remainder of this paper is organized as follows. Section 2 proposes the structural scheme of the HEMA. Section 3 adopts the modified skyhook control strategy for the HEMA to optimize its performance parameters. Section 4 deduces the relationships on the main size parameters of the HEMA on the basis of equivalent magnetic circuit method and optimizes the structural parameters of the HEMA with the goal of electromagnetic thrust force using Ansoft Maxwell software. Section 5 conducts the tests of characteristic and active control on the actuator prototype. Section 6 presents the general conclusions.

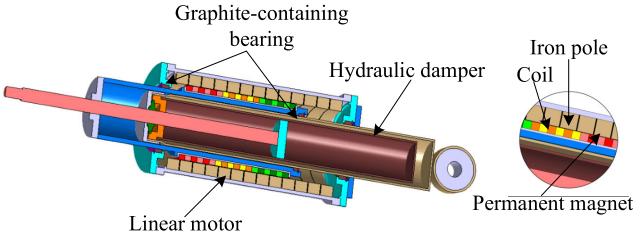

FIGURE 1. Schematic of HEMA.

II. STRUCTURE OF HEMA

Figure 1 shows the schematic of the newly designed HEMA. HEMA is mainly composed of a hydraulic damper and a linear motor. The type of hydraulic damper is ordinary double-cylinder hydraulic damper. The linear motor is a cylindrical PM linear synchronous motor, which comprises a primary part (stator) and a secondary part (mover). The primary part mainly includes iron poles, PM, and external conductor tube. The bottom cover of the external conductor tube is connected with the limit tray of the hydraulic damper, which can make the primary part of the linear motor fixed. Meanwhile, the secondary part includes winding coils, winding casing, and an internal cylinder. The internal cylinder is connected with a piston rod through a flange cover, and graphite-containing bearings are placed on the top and bottom of the internal cylinder, thereby ensuring that the secondary part of the linear motor can follow the movement of the piston rod.

The design of the HEMA includes the following aspects:

1) The PM of the HEMA is axially arranged to obtain a gap flux density higher than that obtained in PM arranged in radial direction [21]–[23]. Moreover, this arrangement has a simpler structure and lower manufacturing cost than the Halbach magnetization. The adjacent PM are separated from highly conductive pole pieces. N42H Nd–Fe–B is used as the PM material, whose remnant flux density is 1.2672 T and coercive magnetic field intensity is 924480 A/m.

2) The mover is slotless. This design increases the thickness of air gap, thereby reducing the magnetic flux density to

make the thrust force ripple smaller than a slotted one. This feature can meet the high dynamic performance requirements of suspension systems.

The working principle of the proposed HEMA is as follows. The upper part of the actuator is connected to the vehicle body through the piston rod. Meanwhile, the bottom part is connected with an axle through the lifting lug. When the vehicle is running, the relative movement between the vehicle body and the axle occurs, thereby making the piston rod of the actuator move up and down in a straight line. Then, the secondary part of the linear motor that is associated with the piston rod moves along with the piston rod. The primary part is fixedly connected with the hydraulic damper and does not move. Hence, relative motion occurs between the PM of the primary part and the winding coils of secondary part. On the basis of the law of electromagnetic induction, the linear motor is equivalent to a generator. The induced electromotive forces are generated in the winding coils. Meanwhile, on the basis of Lenz's law, the electromagnetic damping force is generated while generating the induced electromotive force. The actuator operates in the mode of energy regeneration. In addition, when the three-phase alternating current is inputted into the winding coils and a relative movement occurs between the vehicle body and the axle, which makes the relative motion between the PM of the primary part and the winding coils of the secondary part occur, the linear motor is equivalent to a motor and provides electromagnetic thrust force on the basis of Ampere's rule. The electromagnetic thrust force of the linear motor changes by adjusting the input current. Accordingly, the active force output by HEMA also changes. The actuator also operates in active control mode.

III. PERFORMANCE PARAMETER OPTIMIZATION OF HEMA

The force produced the HEMA mainly includes the electromagnetic thrust force of the linear motor and the damping force of the hydraulic damper. The electromagnetic thrust force provided by the linear motor has a direct influence on the structural parameters of the HEMA. In addition, the damping force is related to the type of hydraulic damper (passive damping coefficient), which also affects the structural parameters of the HEMA. Thus, the electromagnetic thrust force and passive damping coefficient must be confirmed to optimize the structural parameters of the HEMA in Section 4.

When the new HEMA is used for electromagnetic suspension (EMS) and the EMS operates in the active control mode, the HEMA outputs the force used for active control. Therefore, the modified skyhook control strategy for the EMS equipped with HEMA is proposed to determine the electromagnetic thrust force and passive damping coefficient. In comparison with the traditional skyhook control strategy, the EMS introduces a passive damper, and its dynamic model is shown in Figure 2(a).

As shown in Figure 2, when the modified skyhook control strategy is used for the EMS equipped with HEMA,

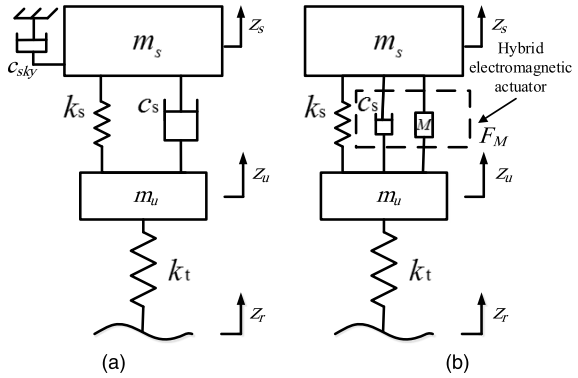

FIGURE 2. Dynamic model of the suspension system: (a) ideal model, (b) actual model.

the hydraulic damper of HEMA acts as a passive damper, and the linear motor is used to track the skyhook damping force. The actual dynamic model of 1/4 EMS based on modified skyhook control strategy is shown in Figure 2(b).

On the basis of Figure 2, the dynamic equations are represented as

$$\begin{cases} m_s\ddot{z}_s = -k_s\left(z_s - z_u\right) + F_M \\ m_u\ddot{z}_u = k_s\left(z_s - z_u\right) - k_t\left(z_u - z_r\right) - F_M \end{cases} \tag{1}$$

Filtered white noise [24] is used as road input and is expressed as

$$\dot{z}_r = -2\pi f_0 z_r + 2\pi n_0\sqrt{G_q\left(n_0\right)v}\cdot w \tag{2}$$

where m_s is the sprung mass; m_u is the unsprung mass; k_s is the spring stiffness; k_t is the tire stiffness; f_0 is the cutoff frequency; n_0 is the spatial frequency; $G_q(n_0)$ is the road roughness coefficient; v is the vehicle speed; w is the white noise; and F_M is the force produced by HEMA, which can be expressed as

$$F_M = -c_{sky}\dot{z}_s - c_s(\dot{z}_s - \dot{z}_u) \tag{3}$$

where c_{sky} and c_s are the skyhook and passive damping, respectively.

Table 1 shows the system parameters.

TABLE 1. System parameters.

Parameter	Value	Parameter	Value
m_s	327.5 kg	f_0	0.1 Hz
m_u	49.4 kg	n_0	0.1 m^{-1}
k_s	19000 N/m	$G_q(n_0)$	2.56×10^{-4} m
k_t	220000 N/m	v	20 m/s

When using the modified skyhook control strategy, the electromagnetic thrust force of the linear motor is used to track the skyhook damping force. A reasonable skyhook damping coefficient must be determined to identify the needed electromagnetic thrust force. Thus, the root mean square (RMS) values of body acceleration, dynamic tire load,

suspension working space, and system energy consumption are taken as evaluation indexes.

$$\|A_{acc}\|_{rms} = \sqrt{\frac{1}{T}\int_0^T \|\ddot{z}_s\|^2\, dt} \tag{4}$$

$$\|F_{dtl}\|_{rms} = k_t\sqrt{\frac{1}{T}\int_0^T \|z_u - z_r\|^2\, dt} \tag{5}$$

$$\|f_{sws}\|_{rms} = \sqrt{\frac{1}{T}\int_0^T \|z_s - z_u\|^2\, dt} \tag{6}$$

Figure 3 shows the influence of skyhook damping coefficient (c_{sky}) and passive damping coefficient (c_{s}) on the evaluation indexes. The skyhook damping coefficient ranges from 0 Ns/m to 20000 Ns/m, whereas the passive damping coefficient ranges from 500 Ns/m to 2500 Ns/m.

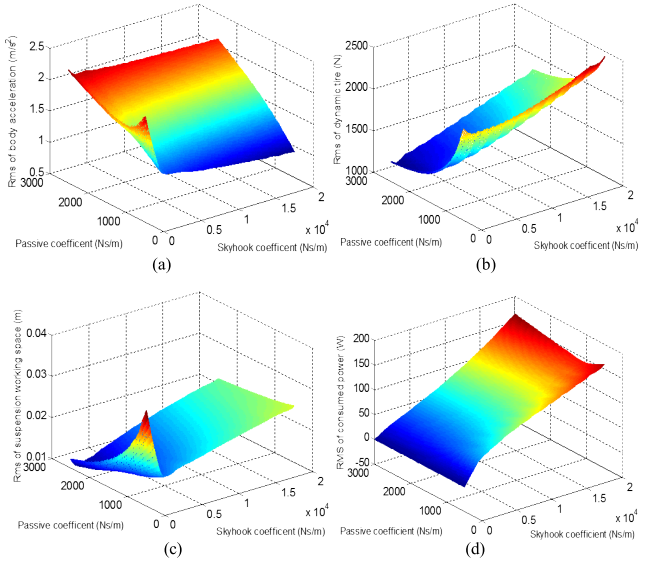

FIGURE 3. Effects of skyhook and passive damping coefficients on the dynamic performance and system energy consumption: (a) body acceleration, (b) dynamic tire load, (c) suspension working space, (d) system energy consumption.

As shown in Figure 3, when the passive damping coefficient is fixed, the RMS of body acceleration decreases with the increase of skyhook damping coefficient, system energy consumption increases with the skyhook damping coefficient, and dynamic tire load and suspension working space decrease and then increase with the increase of skyhook damping coefficient; when $c_{\mathrm{sky}} = 2000$ Ns/m, the minimum value is achieved. When the skyhook damping coefficient is set as a fixed value, the RMS of body acceleration increases with the passive damping coefficient ($c_{\mathrm{sky}} = 0$ is expected), dynamic tire load and suspension working space are opposite, and system energy consumption decreases and then increases with the increase of passive damping coefficient; when $c_{\mathrm{s}} = 1000$ Ns/m, the minimum value is achieved. Thus, $c_{\mathrm{sky}} = 2000$ Ns/m and $c_{\mathrm{s}} = 1000$ Ns/m are set.

Figure 4 shows the electromagnetic thrust force outputted by the HEMA when the skyhook damping coefficient c_{sky} is set as 2000 Ns/m and passive damping coefficient c_{s} is set as 1000 Ns/m.

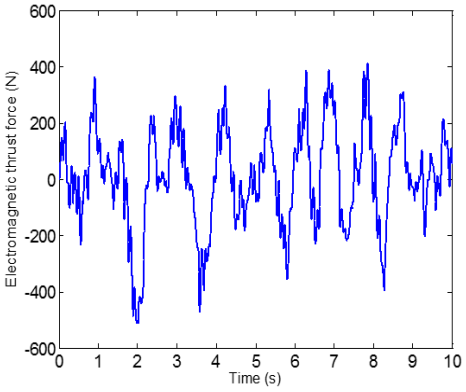

FIGURE 4. Changes of the electromagnetic thrust force.

As shown in Figure 4, when the linear motor tracks the ideal skyhook damping force, the linear motor must provide 513 N of peak electromagnetic thrust force, and the average electromagnetic thrust force is 136.4480 N. Hence, the peak electromagnetic thrust force that the proposed HEMA must provide is set as 520 N.

IV. STRUCTURAL PARAMETER OPTIMIZATION OF HEMA

On the basis of the structure of the proposed HEMA (Section 1), a hydraulic damper is selected as a design basis. Table 2 lists the structural parameters of the hydraulic damper selected for HEMA on the basis of the optimized passive damping coefficient (Section 2) and relevant industry standards.

TABLE 2. Structural parameters of the hydraulic damper.

Working cylinder diameter	Piston rod diameter	External cylinder diameter
27 mm	11 mm	42 mm

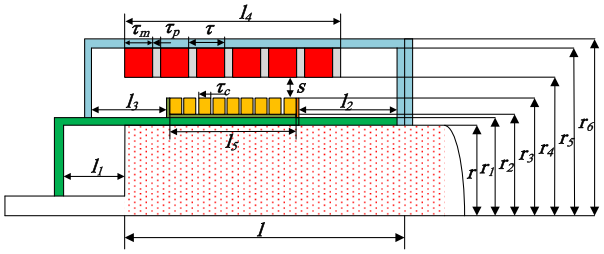

FIGURE 5. Main structural parameters of HEMA.

Figure 5 shows the main structural parameters of HEMA that must be determined. l denotes the length between the upper and the limit tray of the hydraulic damper. When the hydraulic damper is in a static equilibrium position, l_1 denotes the length between the flange cover and the upper part of the hydraulic damper is, l_2 is the maximum bound stroke, and l_3

is the maximum rebound stroke. l_4 is the axial length of the PM, l_5 is the axial length of the coils, τ_m is the thickness of the PM, τ_p is the thickness of the iron pole, τ denotes the pole pitch, τ_c is the thickness of the coil, and s represents the air gap. r is the inner radius of the internal cylinder of the actuator that is equal to the outer radius of the external cylinder of the damper; r_1 is the outer radius of internal cylinder of actuator, r_2 and r_3 are the inner and outer radii of the coil, respectively; r_4 and r_5 are the inner and outer radii of the PM, respectively; and r_6 is the outer radius of the external conductor tube.

The HEMA is designed on the basis of the hydraulic damper; thus, several restrictions for the HEMA design exist. When the hydraulic damper is in a static equilibrium position, the maximum rebound stroke (l_3) is 70 mm, the maximum bound stroke (l_2) is 50 mm, the length between the flange cover and the upper part of the hydraulic damper (l_1) is 70 mm. The length between the upper part and the limit tray of the hydraulic damper (l) is 400 mm. After the linear motor is integrated with the hydraulic damper, the sum of the maximum axial length of PM (l_4) and the maximum rebound stroke and maximum bound stroke should not exceed the length between the flange cover and the limit tray of the hydraulic damper, that is $l_4 + l_3 + l_2 \leq l_{1+}l$. Meanwhile, to ensure that the area of coils does not exceed the magnetic field on the process of movement, the sum of the maximum axial length of coils (l_5) and the maximum rebound stroke and maximum bound stroke should not exceed the maximum axial length of PM, that is $l_5 + l_3 + l_2 \leq l_4$. In addition, the maximum outer radius of the external conductor tube (r_6) is limited by 55 mm. Table shows the design restrictions of HEMA.

TABLE 3. Design restrictions of HEMA.

Parameter	Design restrictions	Description
l_2	≤50 mm	Maximum bound stroke
l_3	≤70 mm	Maximum rebound stroke
l_4	≤350 mm	Maximum axial length of PM
l_5	≤230 mm	Maximum axial length of coils
r_6	≤55 mm	Maximum outer radius of the external conductor tube

However, Table 3 only gives the design restrictions. Thus, the relationships among the main structural parameters of HEMA must be determined by the equivalent magnetic circuit method [23]. Figure 6 shows the equivalent magnetic circuit and the direction of the flux density, where R_m is the magnetic reluctance of the PM, R_p is the magnetic reluctance of the iron pole, R_l is the magnetic reluctance of the external conductor tube, R_s is the total magnetic reluctance of the internal cylinder of the actuator and hydraulic damper, F_C is the magnetic motive force, g is the actual air gap, D_m is the width of the PM, D_Z is the total width of the field of coil and PM, and d is the thickness of the external conductor tube.

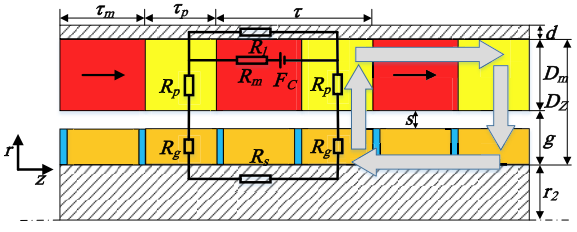

FIGURE 6. Schematic of the equivalent magnetic circuit.

Combined with main structural parameters of HEMA in Figure 5, the relationships of the parameters can be expressed as

$$\begin{cases} r_4 - r_3 = s \\ r_4 - r_2 = g \\ r_5 - r_2 = D_Z \\ r_5 - r_4 = D_m \\ r_6 - r_5 = d \end{cases} \tag{7}$$

On the basis of the type of the previously selected hydraulic damper, the outer radius of the external cylinder of the damper (r) is 21 mm, and the thickness of internal cylinder of the actuator is 4 mm; thus, the outer radius of the internal cylinder of the actuator (r_1) is 25 mm. The thickness of the external conductor tube (d) is 5 mm, and that of the winding casing is 2 mm; hence, the inner radius of the coil (r_2) is 27 mm. The relationships among the width of the PM (D_m), the total width of the field of coil and PM (D_Z), and the thickness of the PM (τ_m) and pole pitch (τ) can be obtained by using the method of equivalent magnetic circuit together with Equation (7). Accordingly, the relationships among the main structural parameters of HEMA can also be obtained.

When using the equivalent magnetic circuit method, the analysis is performed for only one pole pair. The iron pole, internal cylinder of the actuator, and the damper are assumed to have infinite magnetic permeabilities; thus, their magnetic saturations and reluctances are neglected. Moreover, leakage flux is assumed not to exist in the external conductor tube.

Thus, in combination with Figure 6, the relevant magnetic field formulas yield the following:

$$\begin{cases} F_C = H_c \tau_m \\ F_C = \left(R_m + 2R_g\right) \phi_g \\ H_c = \dfrac{B_r}{\mu_0 \mu_r} \\ R_m = \dfrac{\tau_m}{\mu_0 \mu_r \times A_m} \\ R_g = \dfrac{g}{\mu_0 \times A_g} \\ B_g A_g = B_m A_m \end{cases} \tag{8}$$

where H_c is the coercive magnetic field intensity, Φ_g is the air-gap magnetic flux, B_r is the remanent flux density, μ_0 is the permeability of vacuum, μ_r is the relative permeability of PM, A_m is the cross-section area of the magnet, A_g is the lateral area of the pole, B_g is the air-gap flux density, and B_m is the flux density of the PM.

A_m and A_g are expressed as

$$\begin{cases} A_m = \pi \times \left[(r_2 + g + D_m)^2 - (r_2 + g)^2\right] \\ A_g = 2\pi \times \left(d + D_m + \dfrac{g}{2}\right) \times \left(\dfrac{\tau - \tau_m}{2}\right) \end{cases} \tag{9}$$

Different structural parameters can affect the magnetic flux and flux density of air gap, thereby influencing the performance of linear motor and the performance of HEMA. Therefore, on the basis of Equation (8), the relationships among the structural parameters, the magnetic flux, and flux density of air gap are expressed as

$$\begin{cases} \phi_g = \dfrac{B_r \tau_m}{\mu_0 \mu_r \left(R_m + 2R_g\right)} \\ B_g = \dfrac{B_r \tau_m \mu_0 H_c}{\left(2gB_r + \tau_m \mu_0 H_c \dfrac{A_g}{A_m}\right)} \end{cases} \tag{10}$$

On the basis of Equation (10), Figure 7 plots the influence that the ratio of the thickness of the PM to the pole pitch (τ_m/τ) and that of the width of the PM to the total width of the field of coil and PM (D_m/D_Z) have on the magnetic flux of air gap for a single pole pair with a pole pitch.

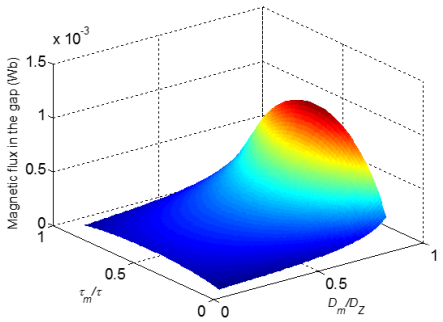

FIGURE 7. Influence of τ_m/τ and D_m/D_Z on the magnetic flux of air gap.

As shown in Figure 7, when D_m/D_Z is fixed, the magnetic flux of air gap increases and then decreases with the increase of τ_m/τ, and when $\tau_m/\tau = 0.5$, the maximum value is achieved. Thus, when optimizing the structural parameters, $\tau_m/\tau = 0.5$ is set to determine the thicknesses of the PM and pole pitch. When τ_m/τ is set as a fixed value, the magnetic flux of air gap increases with D_m/D_Z.

For the HEMA in the passive operating mode, the linear motor is equivalent to an electromagnetic damper, and different structural parameters can affect the equivalent damping coefficient of the linear motor, thereby influencing the performance of HEMA. Thus, when coils are short-circuited, the equivalent damping coefficient of the linear motor produced in a single coil is calculated by

$$C = \frac{B_g^2 \times 2\pi \left(\tau - \tau_m\right)\left(d + D_m + \frac{g}{2}\right) \times (g - s)}{\rho}, \tag{11}$$

where ρ is the resistivity of copper.

On the basis of Equation (11), Figure 8 shows the influence that the ratio of the width of the PM to the total width of the field of coil and PM (D_m/D_Z) has on the equivalent damping coefficient of the linear motor for different total widths of the field of coil and PM.

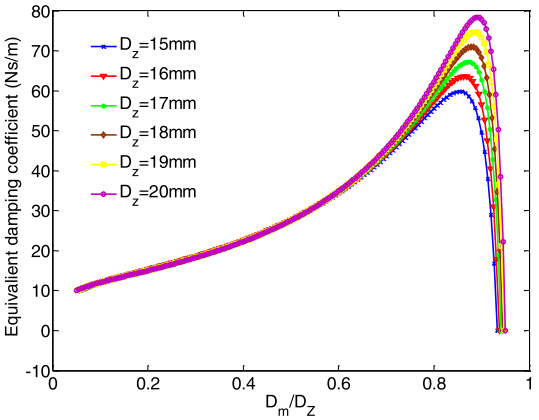

FIGURE 8. Different values of D_Z; influence of D_m/D_Z on equivalent damping coefficient.

For similar total widths of the field of coil and PM, the equivalent damping coefficient of the linear motor increases and then decreases with the increase of D_m/D_Z (Figure 8). When $\tau_m/\tau = 0.8$, the maximum value is achieved. In addition, the peak of equivalent damping coefficient increases with D_Z. However, given $D_Z = D_m + g$, the air-gap thickness (s) as a critical design parameter is set to 1 mm due to manufacturing restrictions. Thus, the ratio of the width of PM to the total width of the field of coil and PM is set as 0.6, that is, $D_m/D_Z = 0.6$.

Therefore, on the basis of the preceding series of analysis, the relationships among the remaining structural parameters can be expressed as

$$\begin{cases} r_3 = 26 + 0.4D_Z \\ r_4 = 27 + 0.4D_Z \\ r_5 = 27 + D_Z \\ r_6 = 32 + D_Z \\ l_5 = 8\tau \\ \tau_c = 8\tau/18 - 0.5 \\ l_5 = 8\tau + 120, \end{cases} \tag{12}$$

where all units of parameters are expressed in mm.

As shown in Equation (12), the pole pitch (τ) and the total width of the field of coil and PM (D_Z) must be determined to obtain the main structural parameters of HEMA. Hence, on the basis of the design restrictions of HEMA in Table 3, the pole pitch cannot exceed 28.75 mm, and the total width of the field of coil and PM should not exceed 23 mm. The pole pitch influences the thickness of PM and the weight of the primary part. Thus, the pole pitch should not be extremely large, and the pole pitch takes the values of 16, 17, 18, 19, and 20 mm. Moreover, the total width of the field of coil and PM can affect the outer radius of the HEMA; thus, it should not be extremely large, so that it will not affect the equipment of HEMA on the vehicle. Thus, the total width of the field of coil and PM takes the values of 16, 17, 18, 19, and 20 mm. On basis of the different values of τ and D_Z, 25 groups of alternative structural parameters of HEMA can be obtained.

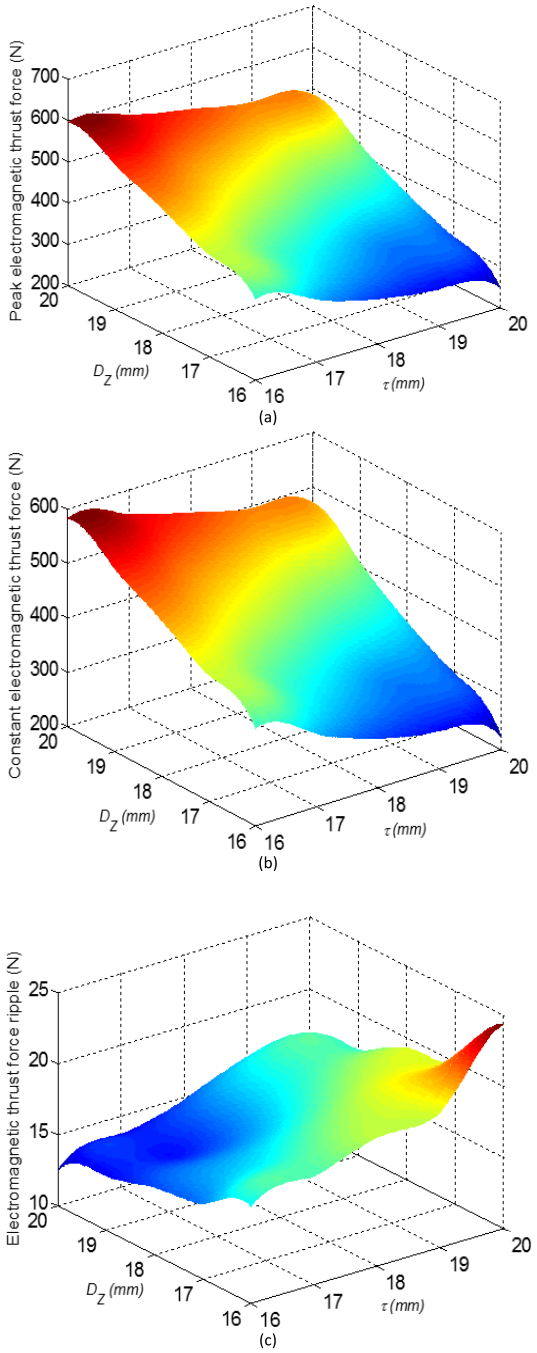

FIGURE 9. Changes in thrust force outputted by HEMA of 25 groups: (a) peak electromagnetic thrust force, (b) constant electromagnetic thrust force, (c) electromagnetic thrust force ripple.

Different structural parameters affect the electromagnetic thrust force output by HEMA [17]–[26]. Thus, the finite element models are established in the Ansoft Maxell software on the basis of the 25 groups of alternative structural parameters. Then, the transient analyses of electromagnetic force are performed on the established finite element models with the goal of peak electromagnetic thrust force (520 N).

Figure 9 plots simulation results of Ansoft Maxwell of the peak and constant electromagnetic thrust force outputted by the HEMA and the electromagnetic thrust force ripple.

From Figure 9, the target requirements of the peak and constant electromagnetic thrust force are considered, making the pole pitch and total width of the field of coil and PM as small as possible to reduce the volume and weight of HEMA; this consideration can reduce the equipment difficulty of HEMA on the vehicle. Moreover, the electromagnetic thrust force ripple is also as small as possible. Consequently, the optimized structural parameters among 25 alternative groups can be obtained, that is, $\tau = 16$ mm and $D_Z = 19$ mm, which correspond to the structural parameters. Table 4 shows the optimized structural parameters of HEMA combined with other known structural parameters.

TABLE 4. Optimized structural parameters of HEMA.

Parameter	Value (mm)	Parameter	Value (mm)
Inner radius of the internal cylinder of actuator r	21	Thickness of coil τ_c	6.6
Outer radius of the internal cylinder of actuator r_1	25	Thickness of iron pole τ_p	8
Inner radius of coil r_2	27	Thickness of PM τ_m	8
Outer radius of coil r_3	33.6	Pole pitch τ	16
Inner radius of PM r_4	34.6	Axial length of PM l_4	248
Outer radius of PM r_5	46	Axial length of coils l_5	128
Outer radius of external conductor tube r_6	51	Air gap s	1

In view of the determined structural dimension of HEMA, the theoretical peak thrust force that can be outputted by the linear motor is 550 N (Figure 10), which can meet the control requirements. Table 5 presents the theoretically achievable basic performance of HEMA.

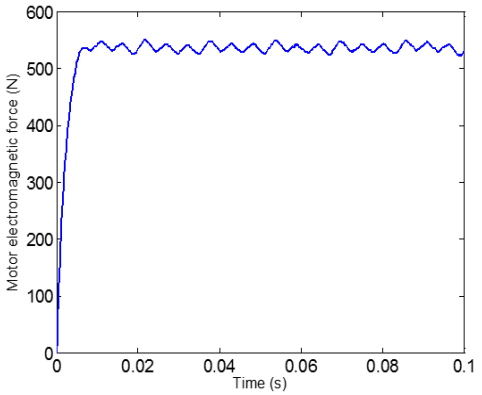

FIGURE 10. Electromagnetic thrust force.

TABLE 5. Theoretically achievable basic performance of HEMA.

Parameter	Value	Description
F_{peak}	550 N	Peak electromagnetic thrust force
F_{RMS}	270 N	RMS electromagnetic thrust force
K_i	73.82 N/A	Thrust coefficient
K_e	59.45 Vs/m	Electromotive force coefficient
Y_{max}	50 mm	Maximum bound stroke
l_{max}	70 mm	Maximum rebound stroke

Figure 11 shows the prototype of HEMA that is developed based on the optimized results. In addition, to verify the effectiveness of the hybrid electromagnetic actuator in improving

(a) HEMA (b) LEMA

FIGURE 11. Prototype.

the dynamic performances of the suspension system, a linear electromagnetic actuator (LEMA) is designed, which represents the current active suspension.

V. BENCH TEST OF HEMA

A bench test, including characteristic and active control tests, is conducted to test the performance of the prototype.

A characteristic test mainly evaluates the damping of HEMA. When HEMA has no external resistance, the linear motors are in a short-circuit state [27], that is, HEMA can form a maximum damping force.

The damping characteristic test uses the sinusoidal input as the excitation source. The amplitude is 50 mm. Figure 12 shows the structural arrangement of the characteristic bench test.

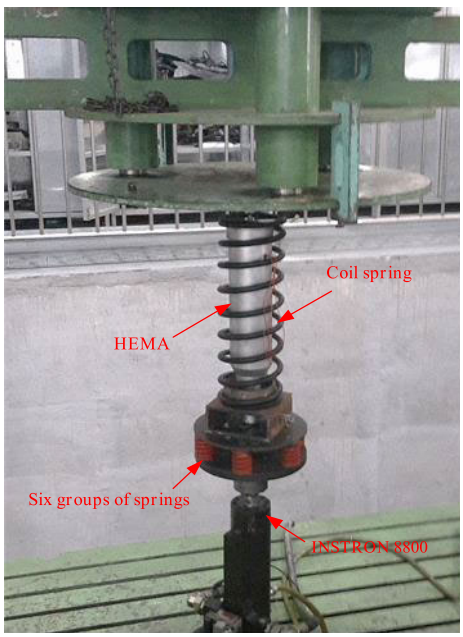

FIGURE 12. Arrangement of characteristic bench test.

Figure 13 shows the damping characteristic of HEMA at different excitation frequencies (velocities).

An active control test is performed to verify the superiority of HEMA in terms of dynamic performance. As shown

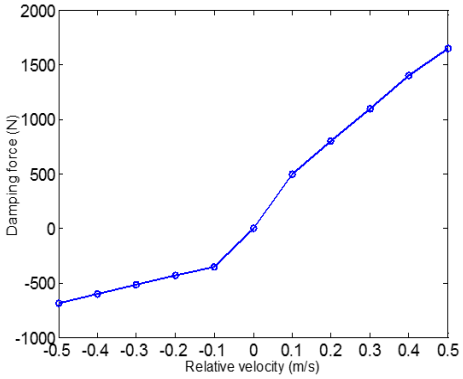

FIGURE 13. Damping force.

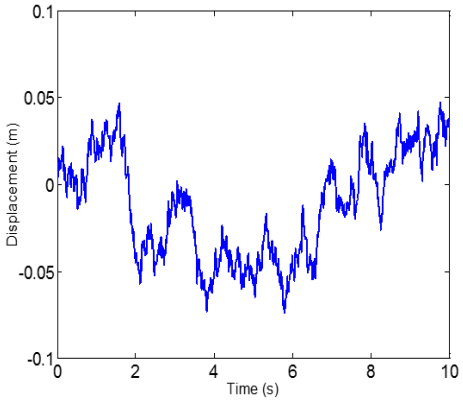

FIGURE 14. Random road excitation.

in Figure 15, an INSTRON 8800 CNC hydraulic servo vibration testing machine is utilized to simulate road excitation (Figure 14), which is the same excitation as simulation analysis. Six groups of springs are used to simulate tire stiffness, and the body acceleration and suspension travel are measured by the acceleration and displacement sensors, respectively. The dynamic tire load can be measured directly

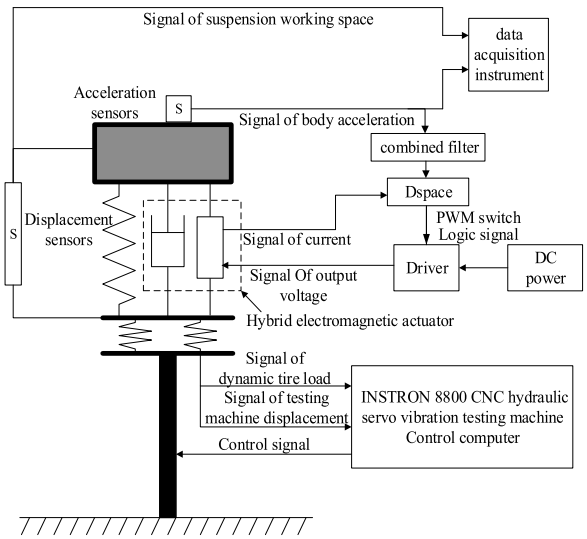

FIGURE 15. Structure of the active control bench test.

by the force sensor equipped by the machine. The hardware circuit of the combined filter is fabricated to transfer the signal of body acceleration to the signal of body velocity that will be inputted to the rapid prototyping controller based on dSPACE. Thus, the desired skyhook damping force can be obtained by the suspension controller. The linear motor is driven by the motor controller to track the desired force.

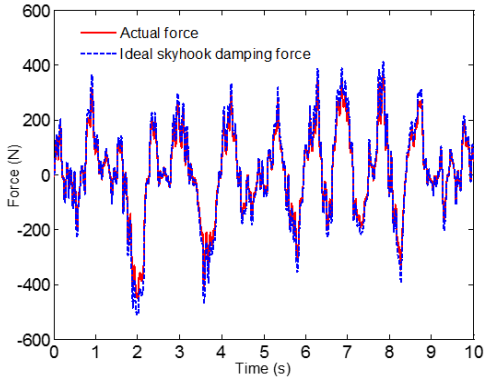

FIGURE 16. Tracking effect of linear motor.

Figure 16 shows a good tracking effect of linear motor. It can be seen that, the actual electromagnetic thrust force outputted by the prototype can track the ideal skyhook damping force well; however, the peak electromagnetic thrust force is less than the maximum ideal skyhook damping force. Analysis yields four main reasons for the error as follows. 1) An error may exist on the process of measuring the signal of body acceleration due to the problem of the experimental instruments. 2) During the development of HEMA, the accuracy of manufacturing is insufficient because of the problems of technologies and materials; hence, the peak electromagnetic thrust force is not reached in terms of theoretical performance. 3) The designed combined filter circuit may be problematic, which results in the error of obtained speed signal. 4) The output electromagnetic thrust force fluctuates during the test due to the edge effect of HEMA.

Figure 17 shows the dynamic performance of HEMA compared with that of passive damper and LEMA from three aspects, that is, body acceleration, dynamic tire load, and suspension working space. Table 6 lists the RMS values of these aspects. It can be seen that, in comparison with passive damper, the body acceleration and suspension working space of HEMA are reduced by 20.6% and 13.3%, respectively, which means the ride comfort is improved. Although the dynamic tire load is increased by 6%, it is in an acceptable range according to the "3σ" rule ($\|F_{dtl}\|_{rms} < 1/3(m_s+m_u)\cdot g$, g is gravitational acceleration, which equals to 9.8 m/s^2). And when compared with LEMA, it can be seen that, although the body acceleration is increased by 2.73%, the suspension working space and dynamic tire load are reduced by 1.1% and 38.1%. Hence, HEMA with modified skyhook control can considerably improve riding comfort and maintain good contact between the wheels and the road. The suspension working space is also in an acceptable range.

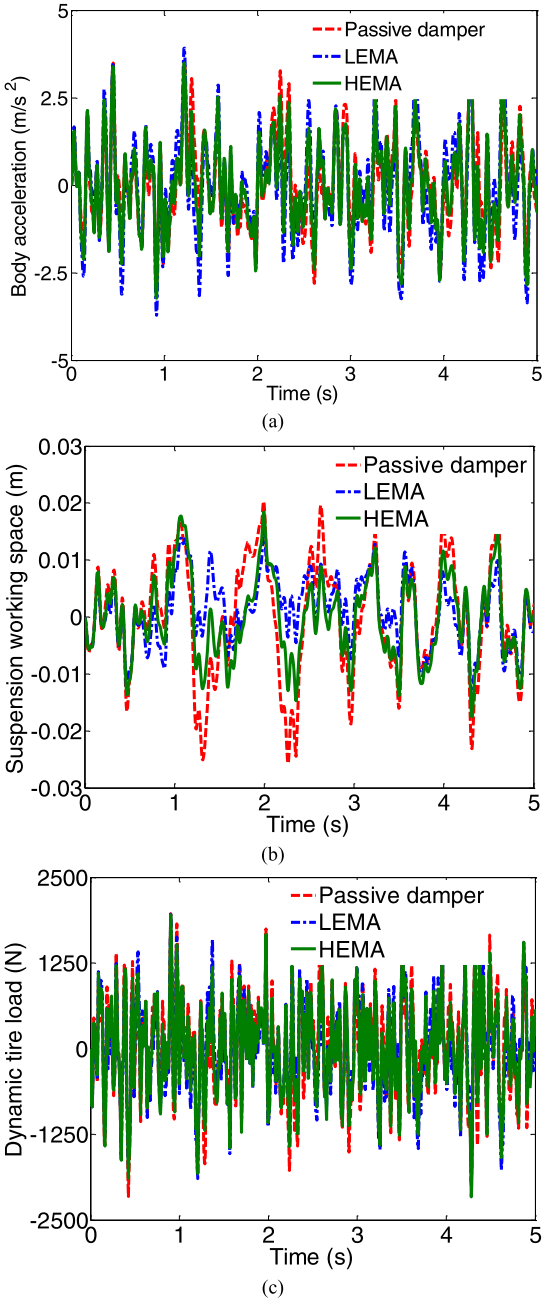

FIGURE 17. Dynamic performance comparison: (a) body acceleration, (b) suspension working space, (c) dynamic tire load.

TABLE 6. Comparison of test results.

Index	Passive	LEMA	HEMA
RMS of body acceleration (m/s^2)	1.89	1.46	1.50
RMS of dynamic tire load (N)	1075.2	1152	1139.8
RMS of suspension working space (m)	0.015	0.021	0.013

Fast Fourier transform is conducted on the preceding time-domain results. Figure 18 shows the power spectral density of the three evaluation indexes. It can be seen from

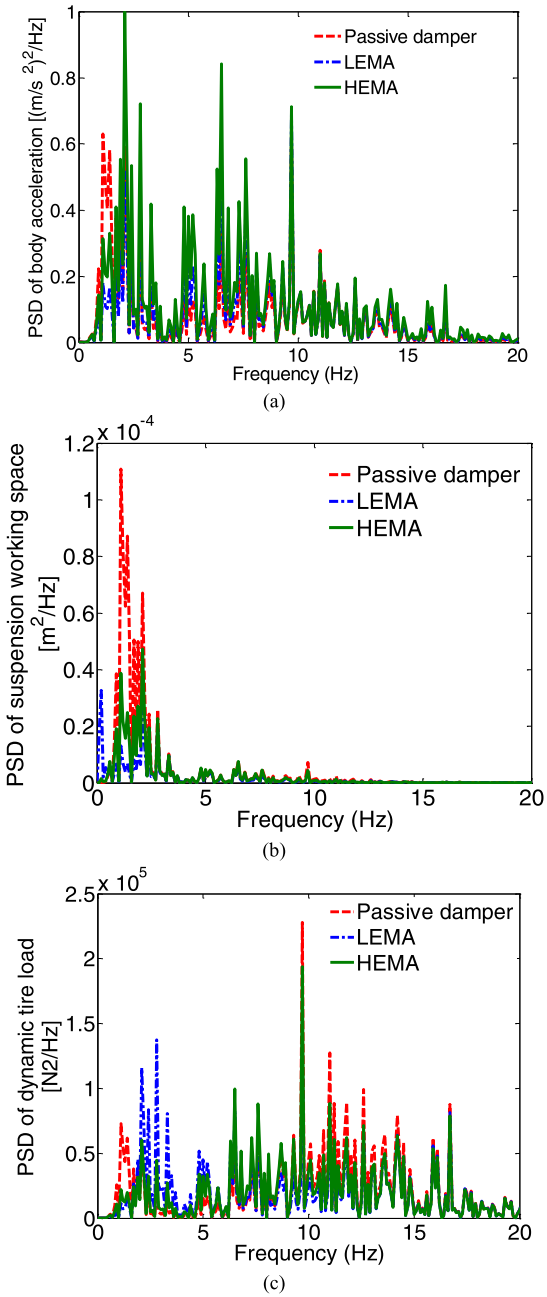

FIGURE 18. **Comparison of results in frequency domain: (a) body acceleration, (b) suspension working space, (c) dynamic tire load.**

the figure that, HEMA can effectively improve the dynamic performance on the body resonance area, and the dynamic performance on the wheel resonance area is not deteriorated.

VI. CONCLUSION

This study integrates a hydraulic damper and a cylindrical PM linear synchronous motor to design a new HEMA. The main conclusions are obtained as follows.

(1) The modified skyhook control is used to match the structure of HEMA. By analyzing the influences of skyhook and passive damping coefficients on the vehicle dynamic performance and system energy consumption, the performance parameters of HEMA are optimized, and the peak electromagnetic thrust force outputted by HEMA is determined.

(2) The relationship between D_{m} and D_{Z} and τ_{m} and τ are obtained using the equivalent magnetic circuit method. Then, the relationships among other structural parameters, D_{Z} and τ, are deduced. The appropriate values of D_{Z} and τ are selected to obtain 25 groups of alternative structural parameters, from which the finite element models are established for analysis. With the goal of peak electromagnetic thrust force that the linear motor must produce, the structural parameters of HEMA are optimized and determined.

(3) On the basis of the optimized results, a prototype of HEMA is developed. The characteristic and active control tests on the prototype are conducted. The results show that the linear motor tracks the desired force effectively. In contrast to the passive damper, the body acceleration and suspension working space of HEMA are decreased by 20.6% and 13.3%, respectively. The dynamic tire load is increased by 16%, which is in a reasonable range. And compared with LEMA, the body acceleration is increased by 2.73%, but the suspension working space and dynamic tire load are reduced by 1.1% and 38.1%, which proves that HEMA with modified skyhook control can considerably improve riding comfort and maintain good contact between the wheels and the road, while keeping the suspension working space in an acceptable range.

REFERENCES

[1] J. Paulides, L. Encica, E. Lomonova, and A. Vandenput, "Design considerations for a semi–active electromagnetic suspension system," *IEEE Trans. Magn.*, vol. 42, no. 10, pp. 3446–3448, Nov. 2006.

[2] R. Ding, R. Wang, X. Meng, and L. Chen, "A modified energy-saving skyhook for active suspension based on a hybrid electromagnetic actuator," *J. Vibrat. Control*, vol. 25, no. 2, pp. 286–297, Jan. 2019.

[3] S. B. David and B. Z. Bobrovsky, "Actively controlled vehicle suspension with energy regeneration capabilities," *Vehicle Syst. Dyn.*, vol. 49, no. 6, pp. 833–854, Jun. 2011.

[4] M. Montazeri-Gh and M. Soleymani, "Investigation of the energy regeneration of active suspension system in hybrid electric vehicles," *IEEE Trans. Ind. Electron.*, vol. 57, no. 3, pp. 918–925, Mar. 2010.

[5] M. Montazeri-Gh, M. Soleymani, and S. Hashemi, "Impact of traffic conditions on the active suspension energy regeneration in hybrid electric vehicles," *IEEE Trans. Ind. Electron.*, vol. 60, no. 10, pp. 4546–4553, Oct. 2013.

[6] M. Montazeri-Gh and O. Kavianipour, "Investigation of the active electromagnetic suspension system considering hybrid control strategy," *Proc. Inst. Mech. Eng., C, J. Mech. Eng. Sci.*, vol. 228, no. 10, pp. 1658–1669, Jul. 2014.

[7] K. Singal and R. Rajamani, "Zero–energy active suspension system for automobiles with adaptive sky–hook damping," *J. Vibrat. Acoust.*, vol. 135, no. 1, Feb. 2013, Art. no. 011011.

[8] Z. Li, L. Zuo, J. Kuang, and G. Luhrs, "Energy-harvesting shock absorber with a mechanical motion rectifier," *Smart Mater. Struct.*, vol. 22, no. 2, Feb. 2013, Art. no. 025008.

[9] Z. Li, L. Zuo, G. Luhrs, L. Lin, and Y.-X. Qin, "Electromagnetic energy–harvesting shock absorbers: Design, modeling, and road tests," *IEEE Trans. Veh. Technol.*, vol. 62, no. 3, pp. 1065–1074, Mar. 2013.

[10] I. Martins, J. Esteves, G. Marques, and F. Dasilva, "Permanent–magnets linear actuators applicability in automobile active suspensions," *IEEE Trans. Veh. Technol.*, vol. 55, no. 1, pp. 86–94, Jan. 2006.

[11] B. Gysen, J. Janssen, J. Paulides, and E. Lomonova, "Design aspects of an active electromagnetic suspension system for automotive applications," *IEEE Trans. Ind Appl.*, vol. 45, no. 5, pp. 1589–1597, Sep./Oct. 2009.

[12] B. Gysen, J. Paulides, J. Janssen, and E. Lomonova, "Active electromagnetic suspension system for improved vehicle dynamics," *IEEE Trans. Veh. Technol.*, vol. 59, no. 3, pp. 1156–1163, Mar. 2010.
[13] B. L. J. Gysen, T. P. J. Van Der Sande, J. J. H. Paulides, and E. A. Lomonova, "Efficiency of a regenerative direct–drive electromagnetic active suspension," *IEEE Trans. Veh. Technol.*, vol. 60, no. 4, pp. 1384–1393, May 2011.
[14] X. Tang, T. Lin, and L. Zuo, "Design and optimization of a tubular linear electromagnetic vibration energy harvester," *IEEE/ASME Trans. Mechatronics*, vol. 19, no. 2, pp. 615–622, Apr. 2014.
[15] B. Ebrahimi, M. B. Khamesee, and M. F. Golnaraghi, "Design and modeling of a magnetic shock absorber based on eddy current damping effect," *J. Sound Vibrat.*, vol. 315, nos. 4–5, pp. 875–889, Sep. 2008.
[16] B. Ebrahimi, M. B. Khamesee, and F. Golnaraghi, "Eddy current damper feasibility in automobile suspension: Modeling, simulation and testing," *Smart Mater. Struct.*, vol. 18, no. 1, Jan. 2009, Art. no. 015017.
[17] B. Ebrahimi, H. Bolandhemmat, and M. B. Khamesee, "A hybrid electromagnetic shock absorber for active vehicle suspension systems," *Vehicle Syst. Dyn*, vol. 49, nos. 1–2, pp. 311–332, Feb. 2011.
[18] M. Ataei, E. Asadi, A. Goodarzi, A. Khajepour, and M. B. Khamesee, "Multi-objective optimization of a hybrid electromagnetic suspension system for ride comfort, road holding and regenerated power," *J. Vibrat. Control*, vol. 23, no. 5, pp. 782–793, Mar. 2017.
[19] E. Asadi, R. Ribeiro, M. Behrad Khamesee, and A. Khajepour, "A new adaptive hybrid electromagnetic damper: Modelling, optimization, and experiment," *Smart Mater. Struct.*, vol. 24, no. 7, Jul. 2015, Art. no. 075003.
[20] E. Asadi, R. Ribeiro, M. B. Khamesee, and A. Khajepour, "Analysis, prototyping and experimental characterization of an adaptive hybrid-electromagnetic damper for automotive suspension systems," *IEEE Trans. Veh. Technol.*, vol. 66, no. 5, pp. 3703–3713, May 2016.
[21] J. Wang, D. Howe, and G. Jewell, "Analysis and design optimization of an improved axially magnetized tubular permanent–magnet machine," *IEEE Trans. Energy Convers.*, vol. 19, no. 2, pp. 289–295, Jun. 2004.
[22] X. Sun, Z. Shi, G. Lei, Y. Guo, and J. Zhu, "Analysis, design and optimization of a permanent magnet synchronous motor for a campus patrol electric vehicle," *IEEE Trans. Veh. Technol.*, vol. 68, no. 11, pp. 10535–10544, Nov. 2019, doi: 10.1109/TVT.2019.2939794.
[23] X. Sun, K. Diao, G. Lei, Y. Guo, and J. Zhu, "Real–time HIL emulation for a segmented–rotor switched reluctance motor using a new magnetic equivalent circuit," *IEEE Trans. Power Electron.*, to be published, doi: 10.1109/tpel.2019.2933664.
[24] Z. Yonglin and Z. Jiafan, "Numerical simulation of stochastic road process using white noise filtration," *Mech. Syst. Signal Process.*, vol. 20, no. 2, pp. 363–372, Feb. 2006.
[25] X. Sun, C. Hu, G. Lei, Y. Guo, and J. Zhu, "State feedback control for a PM hub motor based on grey wolf optimization algorithm," *IEEE Trans. Power Electron.*, vol. 35, no. 1, pp. 1136–1146, Jan. 2020, doi: 10.1109/TPEL.2019.2923726.
[26] X. Sun, K. Diao, G. Lei, Y. Guo, and J. Zhu, "Study on segmented–rotor switched reluctance motors with different rotor pole numbers for BSG system of hybrid electric vehicles," *IEEE Trans. Veh. Technol.*, vol. 68, no. 6, pp. 5537–5547, Jun. 2019.
[27] R. Wang, R. Ding, and L. Chen, "Application of hybrid electromagnetic suspension in vibration energy regeneration and active control," *J. Vibrat. Control*, vol. 24, no. 1, pp. 223–233, Jan. 2018.

XIANGPENG MENG received the B.S. degree in mechanical engineering from Qingdao University, Qingdao, Shandong, China, in 2011, and the M.S. degree in vehicle engineering from Jiangsu University, Zhenjiang, Jiangsu, China, in 2014, where he is currently pursuing the Ph.D. degree in vehicle engineering.

From 2014 to 2016, he was an Assistant Experimentalist. Since September 2016, he has been an Experimentalist with the School of Automotive and Traffic Engineering, Jiangsu University. His research interests include electric vehicle, active suspension, and vehicle system dynamics.

RUOCHEN WANG received the B.S. degree in mechanical engineering from the Luoyang Polytechnic, Luoyang, Henan, China, in 2001, and the Ph.D. degree in vehicle engineering from Jiangsu University, Zhenjiang, Jiangsu, China, in 2006.

From 2006 to 2009, he was a Lecturer, and from 2009 to 2014, he was an Associate Professor. Since July 2014, he has been a Professor with the School of Automotive and Traffic Engineering, Jiangsu University. His research interests include vehicle dynamic performance simulation and control, intelligent vehicle system, new energy vehicle, and electricity generation system of automobile exhaust temperature difference.

RENKAI DING received the B.S. degree in mechanical engineering from the Yancheng Institute of Technology, Yancheng, Jiangsu, China, in 2013, and the M.S. degree in vehicle engineering from Jiangsu University, Zhenjiang, Jiangsu, in 2016, where he is currently pursuing the Ph.D. degree in vehicle engineering. His research interests include active suspension and vehicle system dynamics.

LONG CHEN received the B.S. degree in mechanical engineering from the Jiangsu Polytechnic, Zhenjiang, Jiangsu, China, in 1982, and the Ph.D. degree in vehicle engineering from Jiangsu University, Zhenjiang, in 2006.

He is a Professor with the School of Automotive and Traffic Engineering, Jiangsu University. He is the author of three books, more than 200 articles, and more than 200 inventions. His research interests include dynamic performance simulation and control, intelligent vehicle systems, vehicle operation and transportation planning, and new energy vehicle.